Characterization of a Middle Miocene Monogenetic Volcanic Field Buried in the Canterbury Basin, New Zealand – Part II

Alan Bischoff [a]*, Andy Nicol [a], Andrea Barrier [a] and Hanfei Wang [a]

[a] *Department of Geological Sciences, University of Canterbury, Christchurch, New Zealand*

alanbischoff@icloud.com *corresponding author

This is a non-peer reviewed preprint submitted to EarthArXiv.

It has been submitted on February 13, 2019 to Bulletin of Volcanology.

Characterization of a Middle Miocene Monogenetic Volcanic Field Buried in the Canterbury Basin, New Zealand – Part II

The Maahunui Volcanic Field (MVF) is a cluster of middle Miocene deep submarine volcanoes and shallow intrusions, currently buried by ca 1000 m in the offshore Canterbury Basin, New Zealand. This 'fossil" volcanic system was imaged by high-quality 2D seismic lines and penetrated by the exploration well Resolution-1, which recovered a monzogabbro intrusion and correlative volcanoclastic rocks. In the second part of this study, we present the regional seismic morphological and paleoenvironmental reconstruction of the MVF and adjacent sedimentary strata. Volcanism in the MVF occurred over an area of ca 1,520 km^2, comprising of at least 31 small-volume (< 6 km^3) volcanoes. Reconstruction of the paleo-physiography of the MVF area indicates that eruptions were short-lived and controlled by a plumbing system that fed magma to dispersed eruptive centers, a characteristic of monogenetic volcanic fields. The MVF plumbing system emplaced a number of shallow (< 1000 m depth) intrusive bodies, commonly within Cretaceous-Paleocene sedimentary strata. Saucer-shaped sills are the most typical intrusion-type presenting sizes up to 5 km in width. These shallow intrusions likely have fed magma to some of the volcanoes in the MVF. Eruptions were entirely submarine (500 to 1500 m), most likely producing subaqueous equivalents of maar-diatreme and tuff cone volcanoes. The morphology of the volcanoes is interpreted to be primarily controlled by phreatomagmatic eruptions, in which variations on mechanisms such as water/magma/gas ratio, and on the degree of induration of the country rocks, likely have an important role in the fragmentation and dispersion of ejected material. In addition, post-eruptive degradation has changed the original volcanic morphology, which was controlled by the height and by the position of the volcanic edifices in relation to a late Miocene base-level fall. After volcanism ceased, volcanoes located in a bathyal setting were rapidly buried and preserved, while high volcanoes (> 200 m) located in a neritic setting were likely emergent at the paleo sea-surface. These emerged volcanoes possible have formed an archipelago with at least nine small extinct volcanic islands in the late Miocene. This work provides insights into the complete architecture of volcanic systems within sedimentary basins, which can be applied on the exploration of geoenergy resources such as hydrocarbons and geothermal energy occurring in association with buried and active monogenetic volcanic systems elsewhere.

Keywords: buried volcanoes; monogenetic field; seismic reflection; submarine eruptions.

Introduction

Geological characterization of volcanoes buried in sedimentary basins relies on the interpretation of subsurface geophysical and borehole data (e.g. Holford et al., 2012; Schofield et al., 2016; Penna et al., 2018). The integration of these complementary datasets offer an opportunity to observe the complete architecture and evolution of buried volcanic systems, from emplacement to burial in the host sedimentary basin (e.g. Reynolds et al., 2016; McLean et al., 2017; Bischoff et al., 2017). However, all remote-sensing and borehole datasets have limitations which place constraints on the resulting interpretations. For example, the quality and resolution of seismic surveys are primarily controlled by geophysical parameters such as signal scattering due to changes in rock velocities and densities, energy attenuation with depth, geobody thickness, small lateral continuity relative to signal wavelength, instrumentation limits during seismic acquisition, and computing power (e.g. Abdelmalak et al., 2016; Marfurt, 2018). In addition, boreholes are usually scarce and motivated by a resource exploration, thus, drilling samples and wireline-logs commonly provide little information about the geometries and lateral variations of complex three-dimensional rock bodies (e.g. Planke et al., 1999; Jerram et al., 2009). To fill this information gap, studies have integrated observations from seismic-scale outcrop analogs into the interpretation workflow (e.g. Schofield et al., 2016; Planke et al., 2017; Infante-Paez and Marfurt, 2017). In outcrop, the morphology of volcanoes provide insights into past eruptive styles, edifice growth mechanisms, and cone degradation (e.g. Cas and Wright, 1993; Fornaciai et al, 2012; Kereszturi and Németh, 2013; Silva and Lindsay, 2015), which can help to better constrain the observations from the volcanoes in the subsurface.

Direct comparison between seismic morphology and morphometric analyses of buried volcanoes with observations from outcropping submarine and subaerial volcanoes is a powerful tool for the interpretation of the processes that may have formed the anomalies observed in the seismic data. However, morphometric parameters of distinct volcano-types (e.g. tuff cones, rings, cinders) typically overlap (e.g. Silva and Lindsay, 2015). In addition, volcanic morphology is likely controlled by the interplay of many competing processes, such as steady vs. dynamic mechanisms of fragmentation, fixed vs. variable location of explosion locus, and single vs. multiple eruption phases, which can complicate their interpretation (e.g. Kereszturi and Németh, 2013). This is especially true for buried volcanoes because, in addition to volcanic complexity and limitations of sub-surface interpretation, these "fossilized" volcanoes are likely influenced by superimposed post-eruptive processes (e.g. degradation, compaction, and diagenesis), which can have to alter their original form (e.g. Bischoff, 2019). Because of this, the morphometric parameters of reconstructed buried volcanoes may have application for establishing guidelines for their interpretation and for further investigation of volcanic processes, as long as the limitations of the methods are acknowledged.

In the part I of this study, we introduce the topic and the regional geological setting, explaining the methods and their limitations for characterizing buried volcanoes from seismic and well data, presenting the results from small-scale detailed petrographic analysis, seismic and paleo-environmental interpretation of in the area of the well Resolution-1 (Figure 1 in part I). Here, in the part II, we up-scale interpretations to a regional scale, based on seismic stratigraphic mapping techniques, presenting the seismic morphological reconstruction of the volcanoes on the MVF, and the geological evolution of this volcanic field within the Canterbury Basin.

Data Set, Methods and Limitations

Seismic reflection and well data used in this thesis were sourced from the 2017 New Zealand Petroleum and Minerals petroleum exploration data pack, which includes a large database of reports, maps, wells and seismic surveys loaded in Kingdom© software. We use more than 40,000 km of moderate to high-quality onshore and offshore 2D seismic lines acquired during the 1970s and 1980s, tied to six petroleum exploration and stratigraphic wells drilled in the northern Canterbury Basin (Leeston-1, Clipper-1, Ealing-1, Resolution-1; Charteris Bay-1 and 2; Figure 1 in part I). Seismic line spacing typically ranges from 1 to 8 km, with good vertical resolution up to 6 seconds penetration (ca 5 km) and samples recorded at 0.004-second intervals. The borehole information varies in data-type and quality. Resolution-1 and Clipper-1 contain a more complete dataset that includes lithological, geochemical, geochronological, petrographic and biostratigraphic information from cuttings, cores and wireline logs for the stratigraphic intervals drilled. For this study, detailed petrographic and elemental geochemistry analysis of MVF rocks were conducted on select intervals that could potentially contain Miocene igneous rocks, initially based on the description of the Resolution-1 well from Milne (1975), which is the topic of the first part on this study.

Detailed seismic morphologic characterization (e.g. figure 5 in part I) was conducted for each seismic anomaly that could represent a middle Miocene volcano buried in the study area, and for all anomalies that could represent intrusive bodies within strata of the Canterbury Basin. To recognize which anomalies could date from the middle Miocene, we mapped the pre-eruptive (PrErS) and post-eruptive (PoErS) surfaces of these volcanoes based on seismic volcanic stratigraphy and volcanoclastic occurrences in the Resolution-1 well. To reconstruct the original morphology, edifice heights, and the morphometric parameters at the time of the formation of volcanoes now

buried in the subsurface, three key parameters have to be addressed: i) the acoustic velocity of the material (volcanic and sedimentary rocks) that comprise and enclose the seismic anomalies; ii) the amount of post-eruptive degradation of the edifice before burial; and iii) how much compaction the volcanoes experienced during their burial, from the surface to their actual depth in the basin. Information on the quantification of these parameters is outlined in Bischoff (2019).

We classify the buried seismic anomalies into two main groups: positive and negative morphologies (e.g. Figure 1). Positive morphologies are seismic anomalies characterized by a convex-up shape of PoErS immediately above a relatively flat PrErS horizon (Figure 1A). Negative morphologies are recognizable on seismic lines by pit-like excavations into PrErS (Figure 1B). Next, we sub-classify these anomalies into six classes as positive symmetric cone, positive asymmetric cone, positive trapezium, positive mound, negative funnel-like and negative basin-like. Basal width (W) of positive volcanoes were defined by the horizontal distance between the inflection points of the PoErS horizon in relation to a relatively flat PrErS horizon (Figure 1A). The radius of positive volcanoes corresponds to W/2 or the radius of the steeper flank for asymmetric cones. The width of negative volcanoes was defined as the horizontal distance between the sides of the funnel-like or basin-like structures at the PrErS horizon (Figure 1B). The height and depth (profundity of pit crater excavations) of volcanoes after burial were initially recorded in seconds two-way-time (sec TWT). The height (in TWT) of positive volcanoes was defined as the vertical time-distance between PrErS and PoErS at the apex of the anomaly imaged on 2D lines. The depth (in TWT) of negative volcanoes was measured by the vertical time-wave-transit between the PrErS horizon and the inverse apex of funnel-like or basin-like structures (Figure 1). With the available dataset, we reconstruct the near original morphologies of volcanic

edifices in the MVF. Table 1 shows the parameters, assumption, and limitations used on the seismic morphological characterization and reconstruction of MVF volcanoes. Table 2 shows the equations applied to calculate morphometric parameters of the volcanoes.

Volcanic and Hypabyssal Seismic Facies

We describe five seismic facies interpreted to represent buried volcanoes or hypabyssal bodies in the study area (Figure 2). In this section, we briefly present the main aspects of the seismic facies related with the MVF. Detailed characterization and interpretation of the morphology of intrusions and volcanoes in the MVF are outlined in Bischoff (2019).

Negative Crater-like Disrupted (NCD) are seismic facies characterized by funnel and basin-shaped geometries with shallow to deep excavations into the PrErS horizon. Internal reflectors within these negative anomalies have moderate amplitude, chaotic, disrupted, and sub-parallel at the top of the structure. External reflectors below the PrErS horizon are parallel and semi-continuous. Immediately above the PrErS, a very high amplitude reflector occurs next to the negative anomaly. The amplitude of this reflector decreases with as it increases the distance from the negative anomaly (Figure 2B). The formation of NCD's is likely associated with large phreatomagmatic eruptions, evident from deep pit-like excavations into the PrErS. Further evidence is the laterally related seismic facies that suggest dispersion of material adjacent to the crater-like structure. Both deep excavations and lateral related facies with high disperse material are common features observed in maar-diatreme and tuff ring volcanoes (e.g. Lorenz, V., 1985; White and Ross, 2011). Intense fragmentation of rocks below the PrErS requires considerable energy (e.g Zimanowski et al., 1997; Zimanowski and Büttner, 2003), and it is widely accepted that subaerial basaltic maar-diatremes result from phreatomagmatic eruptions (e.g. White and Valentine, 2016). In addition, the funnel-

like structures in MVF (e.g. Figure 52B) share many morphological similarities with the Foulden Maar imaged by seismic reflection data in the Waipiata Volcanic Field, South Island of New Zealand (Jones et al., 2017). The basin-like geometries maybe correspond to tuff ring volcanoes, however, due to limitations in seismic resolution, this interpretation is uncertain.

Positive Cone, trapezium and Mound-like (PCM) are anomalies characterized by concave downward projections between the PrErS and PoErS horizons, forming seismic morphologies such as mounds, trapeziums and cone-like structures (Figure 2C). In MVF, the central part of PCM's typically show disrupted and chaotic internal facies, which is interpreted to represent a central vent zone. Deposits of the central vent grade laterally to chaotic, semi-continuous and/or inclined reflectors dipping in opposite directions and downlapping onto the PrErS horizon with increasing distance from the vent (Figure 5 in part I), which we interpret to correspond to the flanks of positive volcanoes. These flanks are characterized by a stacked set of seismic reflectors that accumulate near to the interpreted vent zone, which is common stratal relationship observed in submarine and subaerial monogenetic cone-type volcanoes elsewhere (e.g. Cas et al., 1989; Cas et al., 1993; Kereszturi and Németh, 2013; Jutzeler et al., 2014; Reynolds et al, 2016; White and Valentine, 2016). PCM's are interpreted to correspond to submarine equivalents of cone-type dominated volcanoes (apud Kereszturi and Németh, 2013), which can include tuff and spatter cones, formed by the accumulation of tephra above the PrErS and near an interpreted vent. Tuff cones are typical products of phreatomagmatic eruptions (e.g. Kereszturi and Németh, 2013; Silva and Lindsay, 2015), in which block and bomb ballistics, and turbulent jets represent the main mechanisms of particle dispersal and deposition of material (e.g. Cas et al., 1989; Kaulfuss et al., 2012). Spatter cones usually are the products of Hawaiian and

Strombolian eruptions (e.g. Kereszturi and Németh, 2013; Silva and Lindsay, 2015). These volcano-types have been reported in both subaerial and subaqueous environments (e.g. Deardoff et al., 2011; White et al., 2015a; White et al., 2015b; Cas and Giordano, 2014). In MVF, the shallow slope angle (< 16º, details in the subsequent "Volcanic Morphology" section) of the flanks of PCM's suggest that they may correspond to tuff cones, however, the seismic expression of tuff and spatter cones may be difficult to characterize based on morphometric parameters. Thus, we do not discard the occurrence of spatter cones in the MVF. Mound and trapezium-like seismic anomalies are interpreted to represent progressive degradation of cone-like volcanoes (Figure 5 in part I), due to exposure of the cone crest to wave erosion during the 11 Ma fall in base-level (details in section "Eruptive Styles and Edifice Growth Mechanisms").

Saucer High Amplitude (SHA) are high-amplitude reflectors characterized by a saucer-shaped morphology. In cross-sectional view, this seismic facies usually show a sub-horizontal inner sheet parallel to the enclosing strata, and two peripheral inclined sheets cross-cutting the enclosing strata (Figure 2D). This facies is interpreted to correspond to igneous intrusions in sedimentary rocks. They occur in great number in the Canterbury Basin (Blanke, 2010; Barrier et al., 2017), and are described in the literature as saucer-shaped sills (e.g. Hansen and Cartwright, 2006; Holford et al., 2012; Magee et al., 2016), although their contact with enclosing strata typically shows both sill and dike relationships. Minor sills and dike swarms are likely to occur in spatial association with saucer-sills.

Complex Disrupted Cross-cut (CDC) facies are characterized by disrupted reflectors with frequent cross-cutting relationships (Figure 2E). These seismic facies shows internal low-to-high amplitude, continuous to discontinuous, parallel to cross-cutting reflectors. Upper CDC reflectors are usually domed, while lower reflectors have

cross-cutting relationships, which commonly produces loss of seismic reflectivity (e.g. Jackson, 2012; Schofield et al., 2016; McLean et al., 2017). These seismic facies typically occur below eruptive vents and are interpreted to correspond to disrupted blocks of pre-magmatic strata deformed by intrusions, which may be associated with magmatic conduit zones and emplacement of thin (up to 20 m) intrusive bodies.

Tabular Inclined Moderate-amplitude (TIM) are inclined moderate amplitude reflectors with tabular geometries that usually occur below the top basement chronostratigraphic surface. These sub-vertical anomalies are aligned with pre-Cretaceous structures and are commonly located below larger intrusions, or below middle Miocene volcanoes (Figure 2F). They are interpreted as dikes and magmatic conduits that eventually fed intrusions and/or eruptions to the middle Miocene paleo-submarine surface.

Volcano Morphology and Relationship with Intrusions and Diatremes

Volcanic morphology can provide insights about processes such as past eruptive styles, edifice growth mechanisms and cone degradation (e.g. Dohrenwend et al., 1986; Takada, 1994; Tibaldi, 1995; Vesperman and Schmincke, 2000; Martin and Németh, 2006; Corazzato and Tibaldi, 2006; Valentine et al., 2007; apud Fornaciai et al, 2012). To evaluate the syn- and post-eruptive processes that impact the morphology of the MVF volcanoes, we have undertaken a detailed qualitative-quantitative analysis and seismic morphometric characterization for each volcano in the MVF.

We classify the post-burial morphology (i.e. as the volcanoes appear in seismic lines) of 31 individual volcanoes (Figure 3A). Results show that 81% of the MVF volcanoes have a positive morphology, interpreted to represent cone-type dominated volcanoes, while volcanoes that excavate into the PrErS horizon (crater-type dominated) are less frequent. The basal widths (W) of MVF volcanoes range from 550 to 6350 m.

Most volcanoes (22) have a W between 1000 and 3000 m (Figure 3B). The anomalous volcano with W > 6000 m was interpreted from a low confidence seismic anomaly and may correspond to two or three amalgamated and highly eroded volcanoes.

The estimated magnitude of degradation shows that most MVF volcanoes experienced low (<20 vertical meters of erosion) and moderate degradation (20 to 100 m), while seven volcanoes were interpreted to be highly eroded (>100 m). It was not possible to determine the degree of degradation due to the poor seismic quality for five volcanoes (Figure 3C). Most positive volcanoes (25) have overlying domed reflectors or show no evidence of differential compaction, relative to the enclosing siltstones (ca 30% compaction at a depth of 1000; Field et al., 1989). This result suggests that the positive volcanoes have compacted less than or a similar amount to the Tokama siltstone. Only two volcanoes display upper reflectors with “seagull wing” geometries, which suggests that they have compacted more than the enclosing sedimentary strata (Figure 3D). Reconstructed volcanic heights (oHm) vary from 60 to 430 m (Figure 3E) and original slopes (oS) range from 5º to 24º (Figure 3F). Positive cone-like volcanoes mostly range in oHm from 100 to 300 m, with only 16% of the volcanoes outside this range. Slope angles of cone-type volcanoes usually range between 5º and 15.9º (84%). These morphometric ranges are typical of monogenetic volcanoes (e.g. Kereszturi and Németh, 2013; Silva and Lindsay, 2015).

The total depth of negative basin and funnel-like anomalies range between 90 to 230 m (Figure 4A), which is into the morphometric ranges of maar-diatreme volcanoes (e.g. Lorenz, 1985; Kereszturi and Németh, 2013; Silva and Lindsay, 2015). Three of these negative anomalies show small cone-type volcanoes located above them, which could represent intra-crater volcanoes formed by late eruptive events on the top of a larger diatreme structure (Figure 1B). Inter-crater cones are commonly observed in

association with maar-diatreme volcanoes (e.g. Lorenz, 1985; Kereszturi and Németh, 2013). We also evaluate the potential for MFV volcanoes to have formed in association with large intrusions emplaced in lower sedimentary sequences (Figure 4B). Most volcanoes (68%) are likely related to large (> 2 km), shallow intrusions (ca 1 km at emplacement time), suggesting that these igneous bodies could have fed eruptions in the MVF. Typically geometry of this intrusions is saucer-shaped. This deduction is reinforced by petrographic and geochemical interpretation from the igneous rocks in Resolution-1, as presented in the first part of this work. Volcanism fed by intrusion is common in sedimentary basins, with examples observed in southern Australian (Holford et al., 2012; Jackson, 2012; Reynolds et al, 2016) and the North Sea (e.g. Hansen and Cartwright, 2008; McLean et al., 2017).

Paleo-Physiography and Paleo-Environmental Reconstruction

In this section, we extrapolate the observations from the Resolution-1 well to a regional scale, based on seismic stratigraphic analyses in correlation with biostratigraphic data from the Resolution-1, Clipper-1, Leeston-1, Ealing-1, and Charteris Bay-1 and 2 wells, as well as insights from rocks outcropping in the northern Canterbury Basin region (Figure 1 and 2 in part I; Figure 5; Figure 7; Figure 6; Figure 8). The integration of this dataset provides information about the areal distribution of volcanoes within the MVF, and about the external paleo-environments that precede, interact with and post-date the eruptions in the field (Figure 7).

Pre-eruptive stage (priory 12.7 Ma)

During the early Miocene and prior to ca 12.7 Ma (onset of volcanism in the MVF), the northern Canterbury Basin paleo-seafloor was controlled by a low-gradient smooth ramp that gently dipped towards the regional basin depocenter in the SE (Figure

5D; Figure 8), and aligned with the Chatham and Endeavour structural highs (Field et al., 1989; Barrier, in prep). This paleo-physiography is indicated by the chronostratigraphic map presented in Figure 5D, and by the shape of the seismic horizon that represents the early Miocene ramp shown in Figure 8. At the location of the Resolution-1 well, the transition from deep to middle Tokama siltstone (Table 3; Figure 17 in part I) suggests water-depths dropping from deep-lower bathyal to lower bathyal (Table 3), which occurs in association with the unconformity eM, and prior to the onset of MVF eruptions around 12.7 Ma (Figure 5D). Integration of well data and chronostratigraphic indicate that the near pre-eruptive bathymetry of the study area ranges from 500-750 m at its shallowest, and from 1000-1500 m at its deepest segment (red dashed lines in Figure 7).

Syn-eruptive stage (12.7 to 11.5 Ma)

During the volcanic activity, the regional lower bathyal setting remained relatively stable in the MVF area (Figure 8 and 17 in part I; Table 6), however, eruptions and shallow intrusions in the MVF locally raised the paleo-seafloor by ca 12.7 to 11.5 Ma (Figure 17 in part I, Figure 5C). Paleoenvironmental reconstruction of the area enclosing the MVF (Figure 7) shows that by ca 12.5 Ma to 11.5 Ma, water depths range from a minimum of 500 m and maximum of 1500 m deep, which indicate that the MVF eruptions were entirely submarine. However, it is important to remember that the higher the volcanic edifices grow (due to the addition of material on their flanks and tops by successive eruptions), the shallower their summits become. Conversely, these volcanoes are unlikely to have reached the paleo sea-level during their syn-eruptive stage. This is evident by the volcano named pm02, the highest of the shallower edifices (Figure 7). This volcano had an estimated post-eruptive height (oHm) of ca 420 m and was located in water depths certainly > 500 m (Figure 7), which suggests that its

summit was at least 80 m underwater at that time (Table 3). Although our dataset clearly indicates entirely submarine volcanism in the MVF, we cannot discard the possibility of minor subaerial or Surtseyan eruptions had occurred, mainly from volcanoes located in an ultra-proximal setting or from volcanoes not imaged on our seismic dataset.

Post-eruptive stage (11.5 to 11 Ma)

After volcanism ceased around 11.5 Ma, MVF edifices were progressively buried by an increase in sediment influx from the NW, which derived from the early uplift events of a proto New Zealand Southern Alps (e.g. Field et al., 1989). The presence of the extinct submarine volcanic field had a local influence on the distribution of sediments in the area, which is evident by a thick sequence of sediments deposited within the MVF during the erosion and burial stages (Figure 6B). Seismic images show that sedimentation among the volcanic edifices produced a distinctive depositional setting, referred in Bischoff (2019) to as intra-cone plains. We interpret these local cumulative sediment thickness to result from the interplay of increasing NW-derived sediment supply from the Southern Alps and decrease in accommodation space in the MVF area (this last, either by the introduction of volcanic material sourced by the eruptions, or by erosion of the volcanic edifices). Reduction of accommodation space in the north Canterbury Basin may also have been influenced by crustal arching related to the initial stages of Banks Peninsula magmatism (pre-eruptive doming on our volcanic-stratigraphic model; Bischoff et al., 2017), however, further investigation is necessary to test this hypothesis.

By 11 Ma, most volcanoes in the MVF were completely buried in a lower to uppermost bathyal setting (Figure 2A), with the exception of the pc14 and pc09, as both of these volcanoes were partially buried and located in deeper waters (Figure 5B; Figure

6B). Images from seismic lines in the MVF area show that volcanoes proximal to a proto shelf-break have their tops flattened (Figure 5 in part I). This is consistent with the position of unconformity lM, which suggests that these volcanoes experienced degradation due to wave-base erosion and possibly in some cases by subaerial exposure above the 11 Ma paleo sea-level. After 11 Ma, the remaining deep-water volcanoes (pc09 and pc14) were buried by the progressive NW-SE basin-slope progradation, which occurred simultaneously with the establishment of Banks Peninsula in the late Miocene (Figure 8 and Figure 17 in part I; Figure 5A; Figure 6A; Figure 7). Table 3 summarizes the paleogeography and paleoenvironmental evolution in the study area.

Vent Distribution and Eruptive Fingerprint

The isochron map for the MVF active stage (Figure 7) shows the location of cone-type dominated volcanoes mapped in this study. The cluster distribution of individual or overlapping volcanoes provides evidence that the MVF plumbing system fed magma to dispersed eruptive centres (which is characteristic of monogenetic volcanic fields; e.g. Németh, 2010; Kereszturi and Németh, 2013; Németh and Kereszturi, 2015), rather than feeding eruptions at a fixed spot, which is typical of polygenetic volcanoes (e.g. Silva and Lindsay, 2015). Reconstruction of edifices using the morphometric parameters of two volcanoes (pc14 and pc17) with low magnitudes of degradation indicate that about 5.7 km^3 of magma erupted from the pc14 (biggest volcano in the area), and about 1.6 km^3 from pc17 (average size volcano in the area). These volumes are typical for monogenetic volcanoes (e.g. Kereszturi and Németh, 2013; Németh and Kereszturi, 2015; Silva and Lindsay, 2015). Information of the method used to calculate the volumes of buried volcanoes from seismic data is presented in Bischoff (2019).

The seismic reflection fingerprint of the MVF volcanism in the Canterbury Basin differs significantly from observations of long-lived polygenetic volcanoes imaged in seismic surveys offshore Taranaki Basin (e.g. Kora volcano; Bischoff et al., 2017). The transition from light to dark blue colors in the map shows where the amalgamation of PrErS and PoErS occurs, which we interpret as the seismically detected tephra boundary of the MVF (Figure 7). The map in Figure 7 demonstrates that the volcanoes in the MVF characteristically show rapid thinning and amalgamation of the interval between the PrErS and PoErS, with increasing distance from eruptive centers (Figure 2A). This phenomenon is observed for both individual and overlapped volcanoes in the MVF (Figure 7). Subtle thinning indicates that volcanoes of the MVF experienced relatively short-lived eruptive-cycles, compared to background sedimentation rates. Polygenetic buried volcanoes do not show drastic PrErS and PoErS amalgamation with increasing distance from eruptive centers, because the products of volcanism are interbedded and contemporaneous with thicker sequences of basinal deposits (Bischoff et al., 2017), which suggests long-lived volcanism with recurrent eruptive-cycles at a relatively fixed location.

Controls on MVF Morphology

Integration of the results from petrography and seismic reflection analysis allows us to understand that two main processes controlled the morphology of the MVF buried volcanoes: i) eruptive-style, which produced predominately cone and crater-type dominated volcanoes, and ii) post-eruptive degradation of cone-type dominated volcanoes, which is a consequence of the interplay between edifice height and the external paleo-environmental conditions that affect the volcanoes.

Eruptive Styles and Edifice Growth Mechanisms

Results from seismic morphology and petrographic characterization of the volcanoes in the MVF suggest the presence of two main volcano-types: cone- and crater-type dominated volcanoes. Figure 9 shows the main morphologic aspects of these volcano-types along with photos of possible examples of their subaerial equivalents. We opt for comparison to modern subaerial examples because they are better preserved and exposed than outcrops of submarine volcanoes. Despite differences in eruption trigger and edifice growth mechanisms, it is notable that the products of submarine and subaerial eruptions share morphological similarities. Submarine examples that resample subaerial spatter cones, tuff cones, and maar-diatreme volcanoes are common in the literature (e.g. Cas et al., 1989; Jutzeler et al., 2014; Cas et al., 1993; Head and Wilson, 2003; White et al., 2015a; Reynolds et al, 2016). In the following section, we present the main seismic characteristics of cone and crater-type dominated volcanoes of the MVF.

Crater-type dominated volcanoes are characterized by funnel and basin-like depressions into pre-eruptive strata (Figure 52A and B; Figure 9A, Figure 10), likely caused by brittle deformation and mass collapse, and mechanical adjustment of material into a large diatreme (e.g. Lorenz, 1985). The basin-like seismic morphology maybe represents tuff rings, but they are difficult to characterize due to limitations in the seismic resolution of these anomalies. We interpret the funnel-like morphology to be the seismic expression of subaqueous equivalents of maar-diatreme volcanoes based on:

- Large size of excavations into pre-eruptive strata, e.g. 1300 m in width vs. 230 m in depth (see unbedded diatreme in Figure 9A), which indicate intense fragmentation of the host rock below the PrErS (e.g. White and Valentine, 2016);

- Deep craters in association with seismic facies that indicate extensive lateral dispersion of material and deposition at a low angle of repose, ca 2.5 km from the vent, with an average slope dips of 5º increasing to ca 20º near the vent (see tephra ring and tephra plain in Figure 9A);
- Sub-volcanic zone with downward-dipping reflectors, which suggests post-eruptive subsidence and mass adjustment of material into diatremes (e.g. White and Ross, 2011);
- Rock samples from Resolution-1 that suggest intense fragmentation and dispersal processes, which could indicate phreatomagmatic eruptions. This is evident by volcanoclastic rocks with very fine-grained texture, fragments of broken crystals, platy, cuspate and pumice shard shapes, and by the presence of limestone and sandstone lithics (Figure 14 in part I). These lithics are likely derived from lithologies located at the root of the diatremes nf02 and nf03, which are situated ca 3.5 km SW from the well (Figure 4 in part I).

Cone-type dominated volcanoes are represented by upwards deflection of the PoErS horizon above PrErS (Figure 2A and C; Figure 9B, Figure 10). We interpret this morphology to be the seismic expression of subaqueous equivalents of tuff cones. Following, we present the evidence for this interpretation, however, the occurrence of spatter cones and pillow mounds in the MVF is not discarded, although not recognized in this work.

- The occurrence of stacked reflectors sets superimposed onto and above pre-eruptive strata, proximate to a vent (i.e. basal cone, tephra flank and cone apron in Figure 9B);
- Minor excavations into pre-eruptive strata;
- Sub-volcanic zone with upward-dipping reflectors;

- Cone-like morphology with abrupt topographic inflections and average reconstructed slope angles < 16° (i.e. tephra flank in Figure 9B);
- Rock samples from Resolution-1 that suggest explosive eruptions, with products that resemble textures found in deposits of Surtseyan eruptions (e.g. possible armored lapilli and ash aggregates; Figure 15 in part I).

Observations in the MVF show that both cone and crater-type volcanoes have a random distribution in relation to water-depths (Figure 7). Decompression and fragmentation mechanisms at deep-water settings are still mechanisms not completely understood (e.g. Cas and Giordano, 2014; Cas and Simmons, 2018). Observations from the Kermadec island arc suggest a transition from explosive to effusive volcanism around 1000 m water depth (Wright et al., 2006), however, products of explosive eruptions were also reported in water depths above 1000 m (e.g. Clague et al., 2000a; Head and Wilson, 2003; White et al., 2003; Cas and Giordano, 2014; Agirrezabala et al., 2017). Zimanowski and Büttner (2003) argue that subaqueous volcanic thermohydraulic explosions become increasingly improbable at water depths > 100 m, and practically impossible at water depths > 1000 m. However, Clague et al. (2000a) inferred that phreatomagmatic eruptions at the Loihi seamount offshore Hawaii occurred at a minimum depth of 1356 m, which is approximately equivalent to the depth of the root zone of the volcanoes studied here. Cas and Simmons (2018) suggest that subaqueous effusive eruptions can produce fallout deposits of ash-size autoclastic vitric material similar to typical deposits of subaqueous pyroclastic eruptions. This autoclastic process could explain the textures of the volcanoclastic rocks recovered in the Resolution-1 well without necessarily requiring large explosive eruptions. However, autoclastic mechanisms of fragmentation cannot explain the large pit craters excavated into the PrErS horizon, neither the seismic facies that suggests high-energy mechanisms

of fragmentation and dispersion of material (e.g. Lorenz, 1985; White, 2000; Kereszturi and Németh, 2013; White and Valentine, 2016).

The lithological textures presented in the first part of this work together with seismic morphological analysis suggest that the crater-type dominated volcanos in the MVS were likely formed by high-energy explosive eruptions, such as those triggered by phreatomagmatic processes. It is notable that most of the volcanoes in the MVF show a relationship with large intrusive bodies emplaced in organic-rich host rocks. The coeval of thermogenic gases (e.g. CH_4) or CO_2 incorporated into the magmatic system could contribute significantly to the overpressure necessary for these large pyroclastic deep submarine eruptions, as proposed by and Sversen et al. (2004) and Agirrezabala et al. (2017). Biostratigraphic data and paleoenvironmental reconstruction indicate that these large explosions occurred in water-depths ranging from 500 to 750 m at its shallowest, and from 1000 to 1500 m at its deepest part of the MVF. The crucial challenge of modern submarine volcanology is the need to improve understanding of how the different processes of fragmentation, dispersal and deposition of volcanic material are affected not only by changes in hydrostatic pressure, but also by changes in other physical proprieties, such as bulk modulus (deformability vs. compressibility of water), thermal conductivity, heat capacity, the critical point of water, incorporation of thermogenic gases and CO_2 into the magmatic system, and the degree of induration of the country rock (e.g. Kereszturi and Németh, 2013; White et al., 2003; Cas and Giordano, 2014; Agirrezabala et al., 2017).

Post-Eruptive Paleogeography

After the MVF eruptions ceased around 11.5 Ma seismic stratigraphic and biostratigraphic analysis indicates a progressive shallowing in water depths. This event occurs simultaneously with the wake of the basin-slope progradation from NW to SE.

By ca 11 Ma, the MVF can be divided into two halves by the position of a proto shelf-break (Figure 7). The shallower NW part of the area was located in a neritic environment (< 200-400 m), while the deeper SE part remained in an uppermost bathyal setting (> 200-400 m). Volcanoes with oHm >200 m and located proximal to the 11 Ma proto shelf-break show increasing amounts of degradation (e.g. flattened-tops relative with the lM unconformity, reflectors downlaping from the edifice into basin strata), while volcanoes located distal to the proto shelf-break were buried and well preserved independently of their reconstructed post-eruptive height (Figure 11, Figure 12, Figure 13). In addition, volcanoes classified to have had a low amount of degradation always show a cone morphology, independent of external paleo-environmental factors, while highly degraded volcanoes are always located proximal to the proto shelf-break position (Figure 7), which suggest that their tops may have been eroded.

These eroded volcanoes typically show trapezium and mound seismic morphologies. Buried mounds show H:W ratio < 0.05, while trapezium and cone-like volcanoes have H:W ratios between 0.058 and 0.172. We observe that H:W shows inverse proportionality with the degree of estimated degradation (Figure 12), which reinforces the relationship between the amount of degradation and volcanic morphology. Therefore, the higher degree of degradation gives a lower H:W ratio which we interpret to produces the mounds and trapezium-like morphologies from an original cone-like morphology. Clague et al., (2000b) demonstrate that flat-topped cones in Hawaii can form as continuously overflowing lava ponds. This situation is unlike to explain the flatten-tops of the MVF cone-type dominated volcanoes because the accumulation of lava deposits typically form high-amplitude reflectors in seismic data (e.g. Planke et al., 1999; Holford et al., 2012; Reynolds et al., 2017). In addition, the volcanoes with “flatten-tops” in MVF always have their tops associated with the lM

unconformity. We interpret that some originally high cone-like volcanoes could have emerged above sea-level during the late Miocene sea-level drop and experienced degradation by wave erosion. These emergent extinct volcanoes may have formed an archipelago of at least nine small volcanic islands by ca 11 Ma (Figure 7).

Conclusions

Volcanism in the Maahunui Volcanic Field (MVF) occurred over an area of ca 1,520 km^2, comprising of a cluster of at least 31 middle Miocene volcanoes. These volcanoes are currently buried by around 1000 m of sedimentary strata in the offshore Canterbury Basin. Representative products of this volcanism are basaltic (possibly alkaline) in composition. Volcanic edifices typically had small-volume (< 6 km^3) immediately after their eruptive phase. Reconstruction of the paleo-physiography of the MVF area indicates that eruptions were short-lived and controlled by a plumbing system that fed magma to dispersed eruptive centers, a characteristic of monogenetic volcanic fields. The MVF plumbing system emplaced a number of shallow (< 1000 m depth) intrusive bodies, commonly within Cretaceous-Paleocene sedimentary strata. Saucer-shaped sills are the most typical intrusion-type presenting sizes up to 5 km in width. This shallow intrusions likely have fed magma to some of the volcanoes in the MVF. Eruptions were entirely submarine (500 to 1500 m), most likely producing subaqueous equivalents of maar-diatreme and tuff cone volcanoes. The morphology of the volcanoes is interpreted to be primarily controlled by phreatomagmatic explosions in which variations in the eruptive mechanisms such as water/magma ratio and the mechanical behavior of the pre-eruptive substrate likely have an important role in the fragmentation and dispersion of ejected material. However, the occurrence of spatter cones and pillow mounds in the MVF is not discarded, although not recognized in this study. In addition, post-eruptive degradation has changed the original volcanic

morphology, which was controlled by the height, and by the position of the volcanic edifices in relation to a late Miocene base-level fall. After volcanism ceased, volcanoes located in a bathyal setting were rapidly buried and preserved, while volcanoes located in a neritic setting and with edifice heights > 200 m were possibly emergent at the paleo sea-surface. These emerged volcanoes possible have formed an archipelago with at least nine small extinct volcanic islands in the late Miocene. Understanding the relationship of these diverse volcanic and sedimentary processes contribute with insights into the complete architecture of buried volcanoes, which is important to assess the risks, and to improve the likelihood of finding commercially viable geoenergy resources such as hydrocarbons and geothermal energy in association to buried and active monogenetic volcanic systems elsewhere.

Table 1: Attributes and parameters used on the seismic morphological characterization and reconstruction of MVF volcanoes.

Seismic morphometric parameters	Shape of the anomaly after burial, basal diameter (m), height after burial (s) for cone-like anomalies, depth after burial (s) for crater-like anomalies.
Assumptions and estimations	Post-eruptive degradation, degree of compaction during burial, seismic wave velocity (m/s) within the anomalies. See Bischoff (2019) for details.
Other considerations	Seismic data quality, position of the 2D seismic line relative to the center of the seismic anomaly, cone-like anomalies associated with underlying funnel-like anomalies, evidence for large intrusions underneath anomalies, paleo-geographic position relative to major base-level falls, the presence of canyons that may have eroded part of the anomalies, seismic facies that indicate proximal deposits that may have been eroded from the anomalies.

Table 2: Equations used to calculate seismic morphometric parameters of the MVF volcanoes.

Abbreviations	Equations
HaBs: height after burial in seconds **Vel:** estimated acoustic velocity in m/s **HaBm:** height after burial in meters **comp:** estimated amount of compaction (%) **HbBm:** height before burial in meters **degr:** estimated amount of degradation in meters **oHm:** estimated original eruptive height in meters **W:** basal width **Rt:** basal radius **HW:** height vs. basal width ratio **oS:** estimated eruptive flank slope **atan:** arc cotangent	$HaBm = \frac{HaBs \times Vel}{2}$
	$HbBm = HaBm + (HaBm \times comp)$
	$oHm = HbBm + degr$
	$HW = \frac{oHm}{W}$
	$oS = 180^0 \times \frac{\mathrm{atan}(oHm/Rt)}{\pi}$

Table 3: Main stratigraphic and paleoenvironmental characteristics of the MVF area. Interval highlighted in red corresponds to the active eruptive time in the volcanic field.

Age	Physiography	Magmatic stage	Depositional setting	NW shallower	SE deeper
11 Ma and younger	Slope and basin morphology	Complete burial	Neritic to uppermost bathyal	100 to 200 m and progressively shallower	200 to 400 m and progressively shallower
Post-degradational surface (unconformity lM) and rapid progradation					
11.5 to 11 Ma	Onset of slope-and-basin morphology (proto shelf-break)	Degradational and part of the burial	Uppermost bathyal to mid bathyal	200 to 400 m (volcanoes ≥ 200 m exposed to sea-level)	600 to 800 m (≥ 100 m at volcano summits)
Post-eruptive surface and onset of progradation					
12.7 to 11.5 Ma	Ramp, rugged at MVF location	Syn-eruptive	Lower bathyal	500 to 750 m (≥ 80 m at volcano summits)	1000 to 1500 m (≥ 200 m at volcano summits)
Pre-eruptive surface					
Early Miocene and priory to 12.7	Smooth ramp	Pre-eruptive	Lower to deep bathyal	1000 to 1500 m	1500 to 2000 m

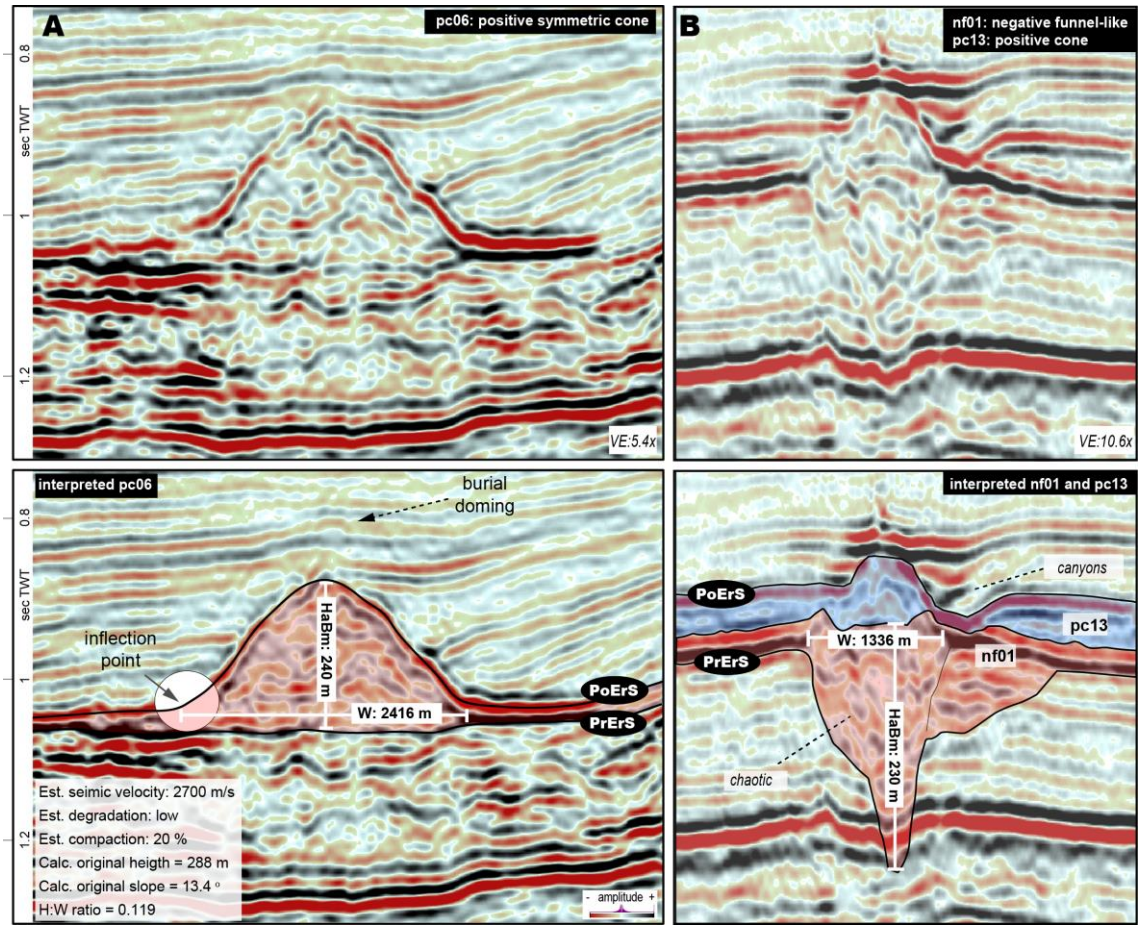

Figure 1. Seismic morphometric measurements and example of morphology classification of MVF volcanoes. A) Shows a positive symmetric cone (cone-type dominated). B) Shows a compound morphology. Bottom part (nf01 in light red) has a negative funnel-like shape (crater-type dominated) and its lateral association. Upper part (pc13 in light blue) shows a positive asymmetric cone shape (cone-type dominated) and its lateral association. Note that pc13 have one of the flanks eroded by canyons.

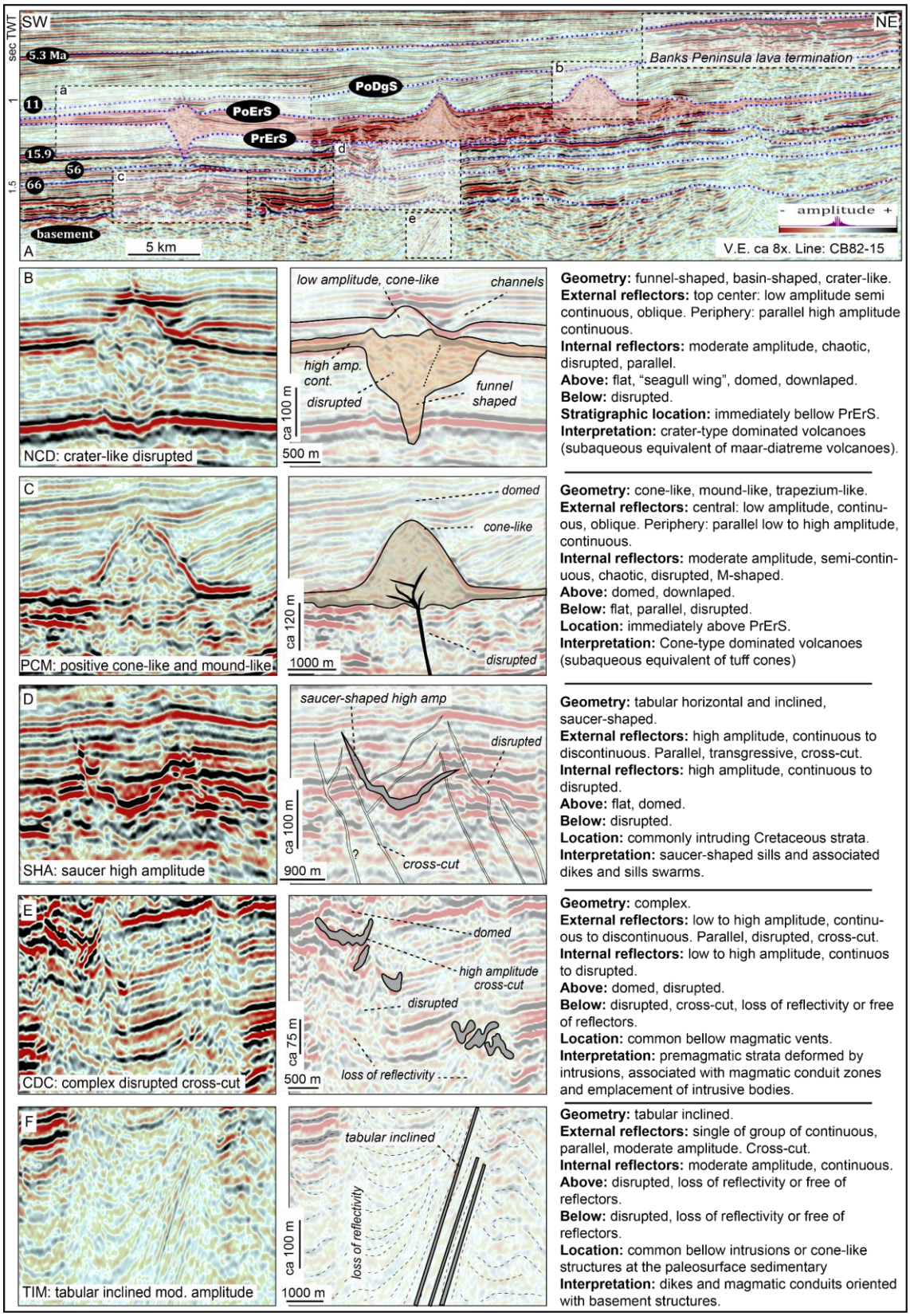

Figure 2. Igneous seismic facies in the study area. A) Regional 2D strike/oblique seismic section showing the lower (PrErS) and upper (PoErS) stratigraphic limits of the

MVF (see chapter 4.5.5 for details). B and C show images interpreted as volcanoes erupted in the MVF, while figures D, E and F show images of interpreted intrusions.

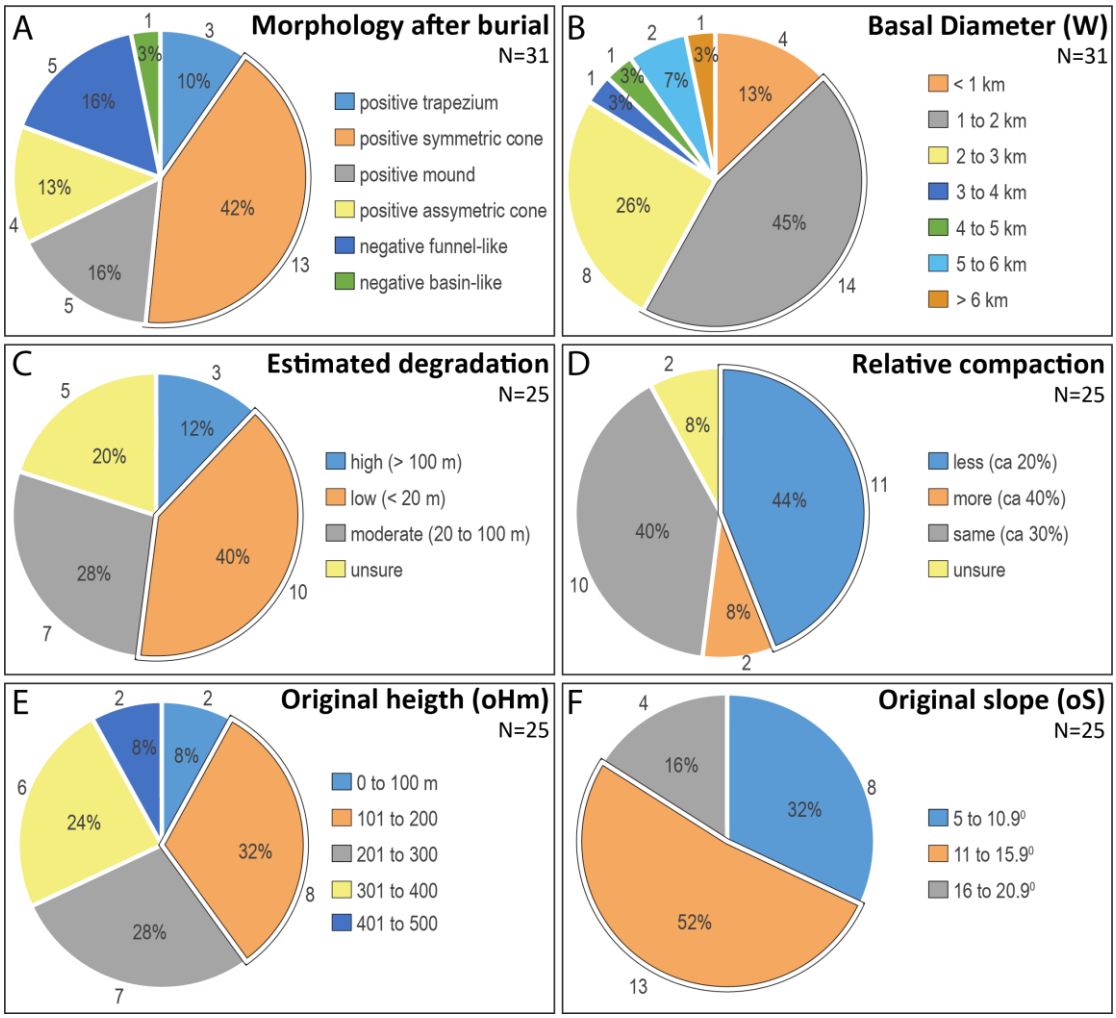

Figure 3: Pie diagrams showing the qualitative-quantitative morphometric results from MVF volcanoes. See text for details.

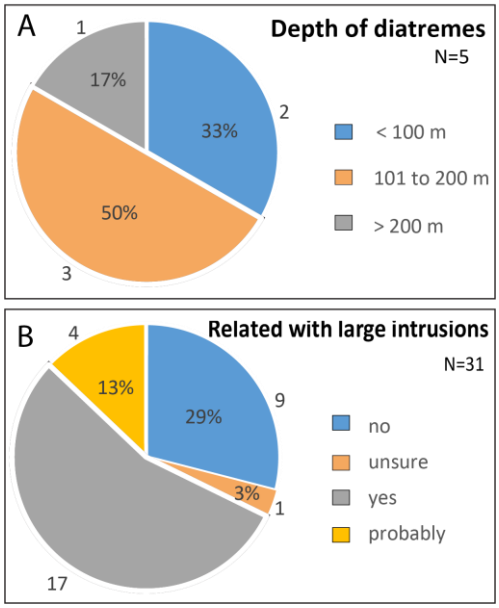

Figure 4: Pie diagrams showing the depth of diatreme craters (A), and number of volcanoes interpreted to be underlain by large (> 2 km) and shallow (ca 1 km) intrusions (B).

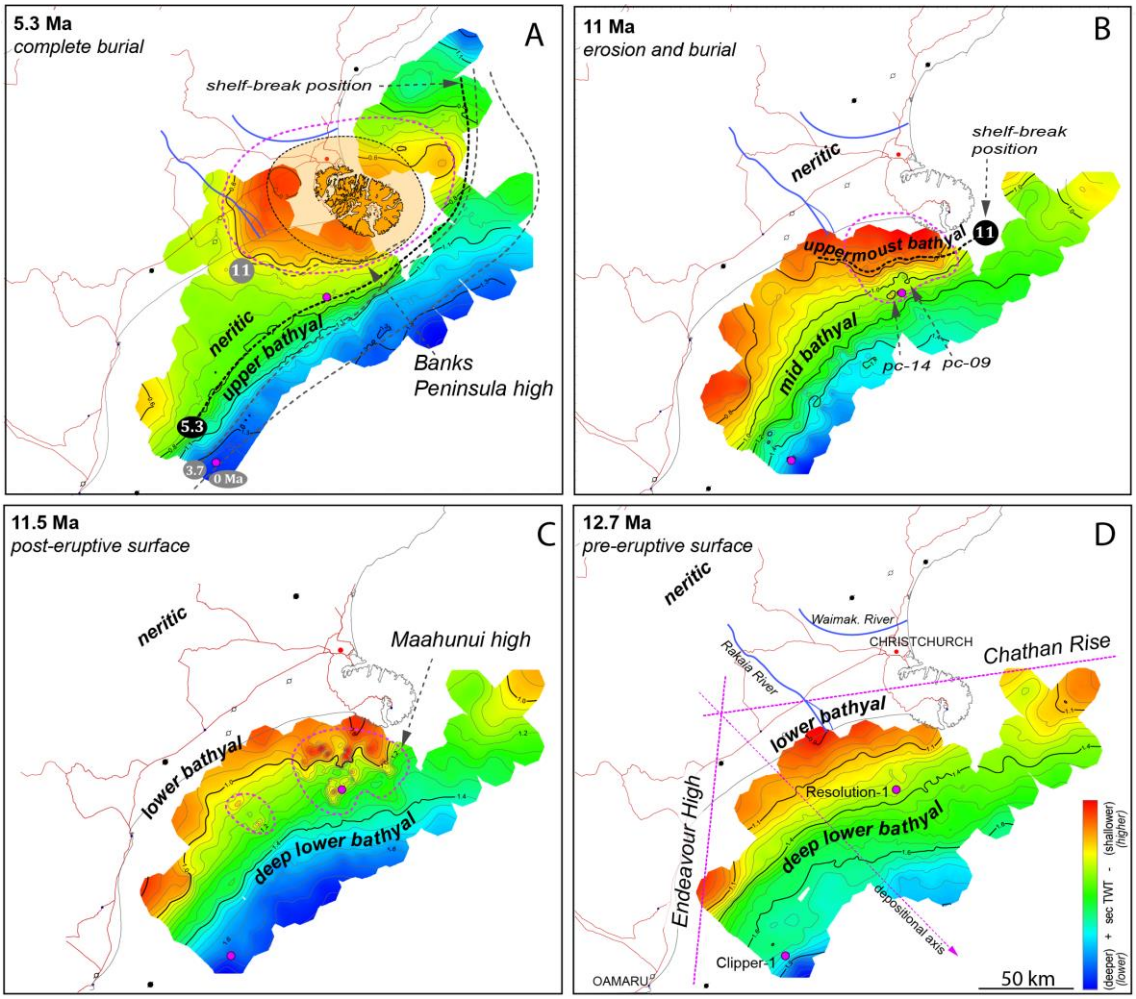

Figure 5: Chronostratigraphic maps of the northern Canterbury Basin. The MVF erupted entirely in a lower bathyal setting (D and C) and was buried in a lower to uppermost bathyal setting (B) due to rapid SE sediment progradation in the northern Canterbury Basin. During the Neogene, the physiography of the basin evolved from a ramp to a basin-slope morphology (C to A). Outcropping paleo-environments compiled from Field et al. (1989).

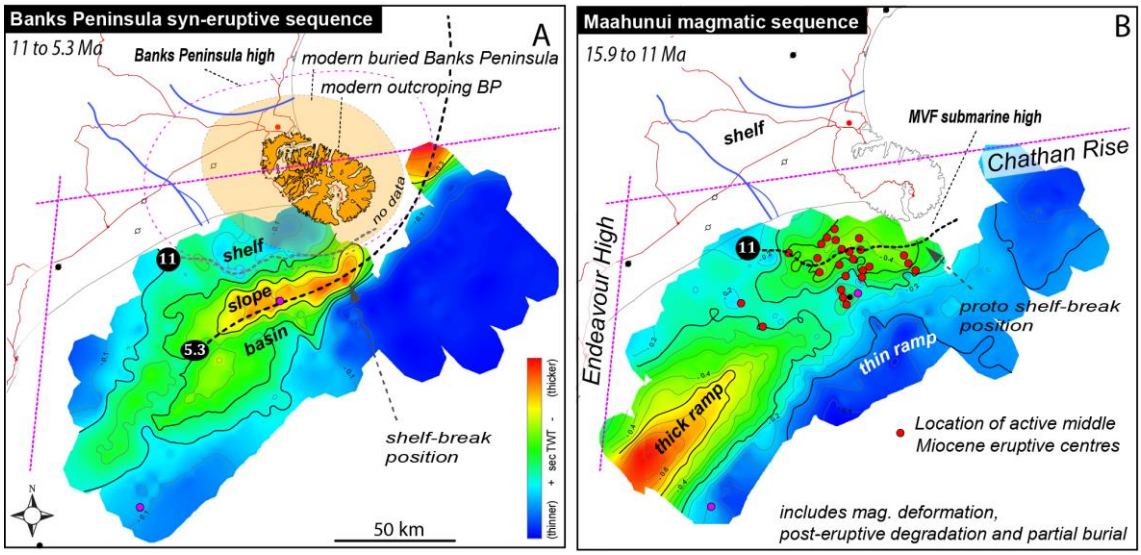

Figure 6: Isochron maps of the northern Canterbury Basin. By 11 Ma and younger, most volcanoes were buried by the slope progradation associated with increasing sediment supply from the NW (A), simultaneously with the installation of the Banks Peninsula. Note in (B) that a thicker pile of sediments were deposited at the location of the edifices of the MVF during their erosion and partial burial (i.e. MVF submarine high).

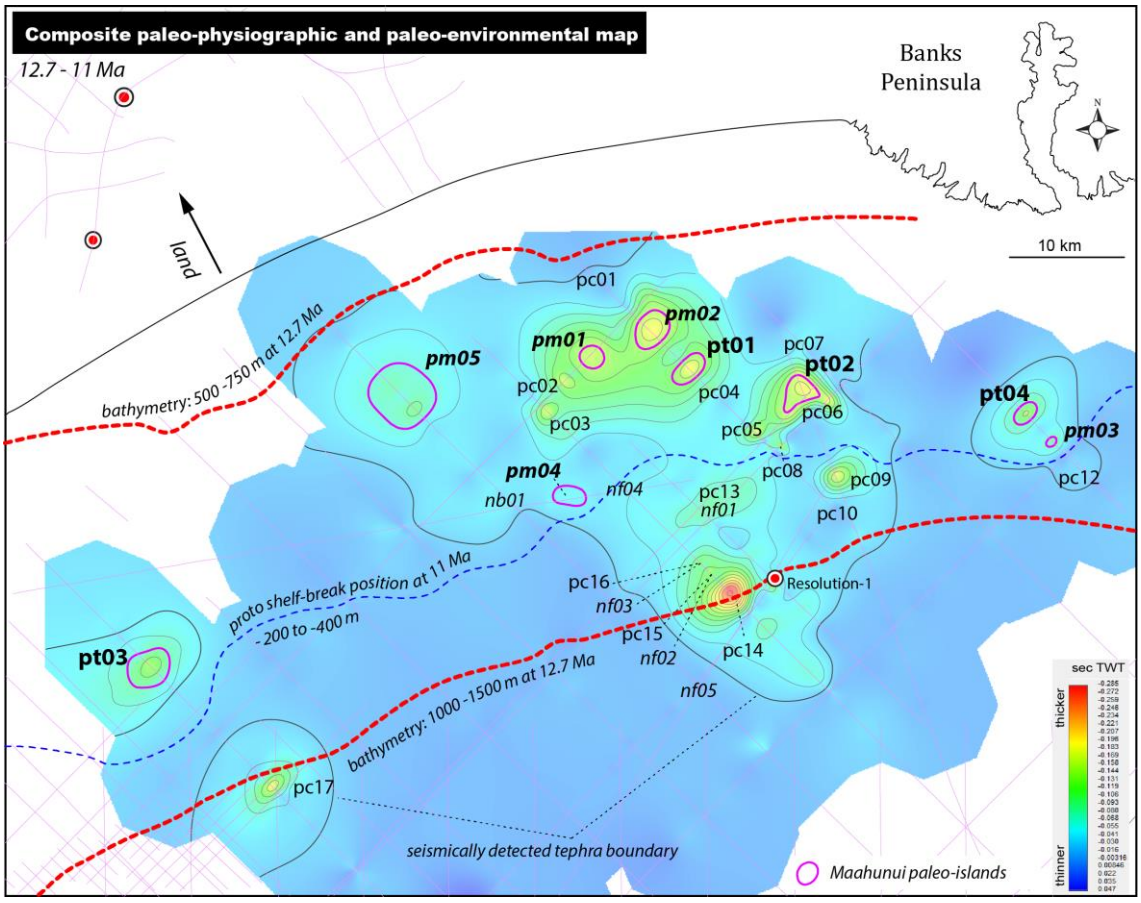

Figure 7: Composite paleo-physiographic and paleoenvironmental map of the study area from ca 12.7 to 11 Ma. Abbreviations are plotted at the position of MVF volcanoes and correspond to their morphology. Pc's are positive cones, pt's are positive trapezium, pm's are positive mounds, nf's are negative funnel-like structures and nb's are negative basin-like seismic anomalies. Red dashed lines show the approximate bathymetry at the onset of eruptions in the MVF. Blue dashed line shows the position of the shelf-break at 11 Ma. Note that all pm's and pt's are located within relatively shallower waters, proximal the 11 Ma shelf-break. Note that volcanoes distal the 11 Ma proto-shelf break shows a sharp increase in slope towards their summit, while volcanoes located proximal to this line show shallower slopes. We interpret that volcanoes highlighted in purple correspond to an ancient archipelago comprising nine small extinct volcanic islands. Details of the construction of this map are presented in Bischoff (2019).

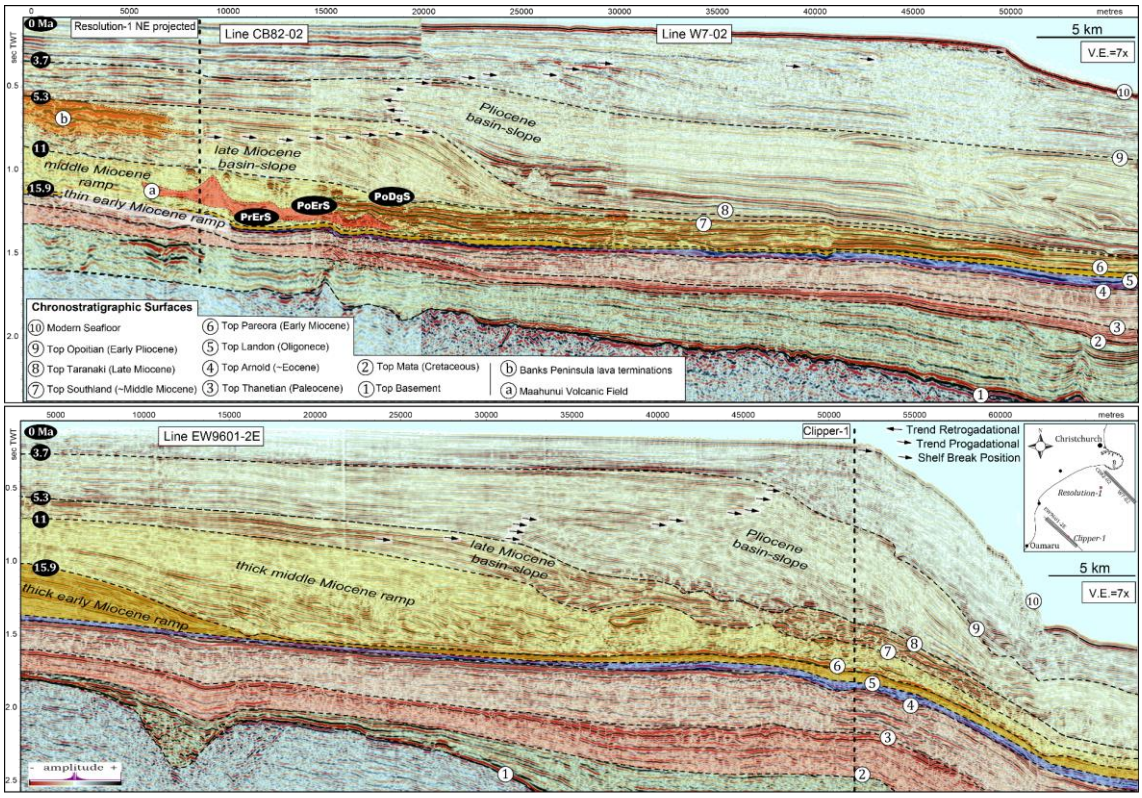

Figure 8: 2D seismic lines showing the location of the MVF in relation to the regional chronostratigraphic horizons mapped in the study area, from the Cretaceous to Recent, and the main physiography of the basin. Neogene to Recent shelf-break migration is indicated by arrows that show the location of the shelf-break at each time, with the arrowhead pointing in the direction of migration.

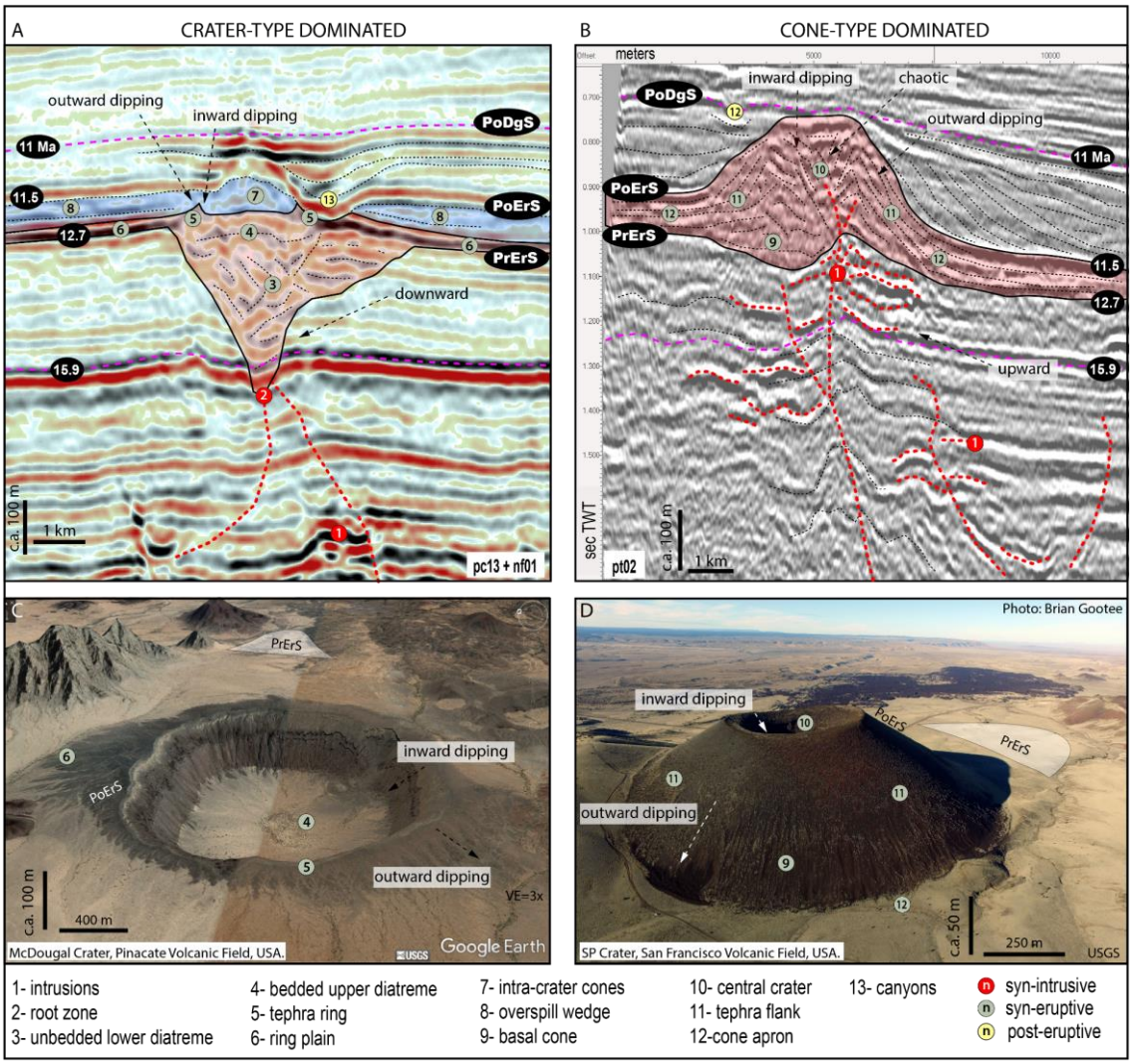

Figure 9: Top images show 2D seismic sections of a crater (left) and a cone (right) type dominated volcanoes. In the seismic sections, crater-type is characterized by deep funnel-like excavations into the PrErS horizon, while cone-type is characterized by upwards deflection of the PoErS above the PrErS and reflectors that pile-up above PrErS. Bottom images correspond to interpreted subaerial analogs. The crater-type is a classic maar-diatreme volcano (McDougal Crater, in the USA), while the cone-type is a well-known scoria cone (SP Crater, USA). Despite morphometric differences and distinctive edifice growth mechanisms, tuff cones and scoria cones share many morphologic similarities, such as the presence of a crater zone with layers inward dipping, and peripheral flanks with layers outward dipping. Note the geometric similarity between the volcanoes in seismic and analog images. Further details and interpretation of the architecture of these volcanoes are presented in Bischoff (2019).

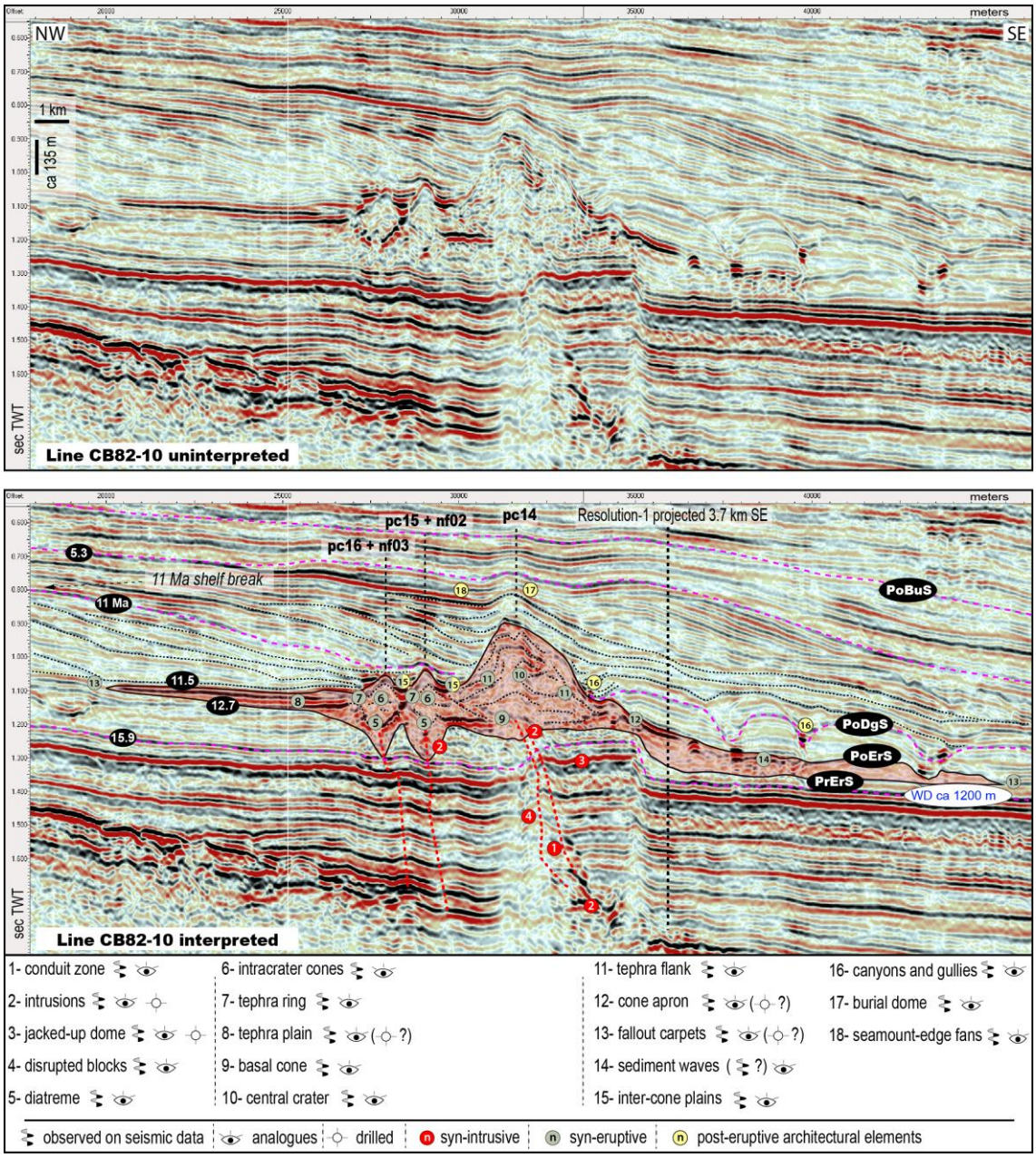

Figure 10: Uninterpreted (above) and interpreted (below) 2D seismic line showing the main architectural elements related to cone-type volcanoes in the MVS volcanos. Numbers in red dots are syn-intrusive architectural elements, in green syn-eruptive, and in yellow post-magmatic architectural elements (detail architectural characterization is presented in Bischoff (2019). Based on seismic stratigraphic interpretation, the lower sequence of volcanoclastics recovered in Resolution-1 was probably sourced from volcanoes NW or W of the well (likely nf02 and nf03). Tuffs from -1103 to -1110 m depth were likely vented from pc14. WD is the interpreted approximate water depth at the time of the formation of these volcanos.

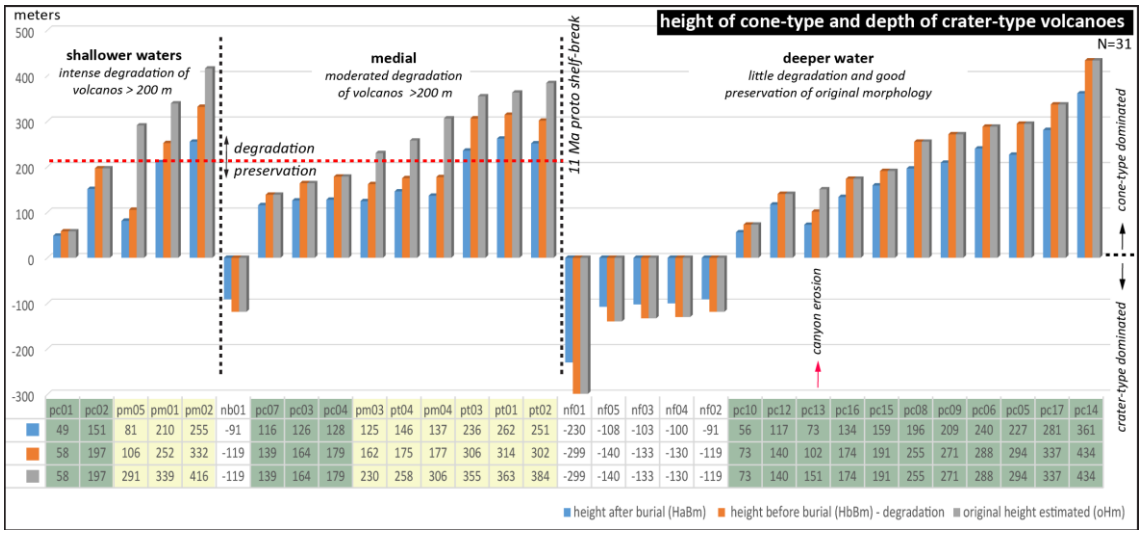

Figure 11: Morphometric analysis of MVF volcanoes relative to their post-eruptive paleo-environmental location (11 Ma). Blue bars show the height of volcanoes after burial (HaBm). Orange bars show decompacted height values (HbBm). Grey bars show reconstructed original height of the MVF volcanoes (oHm). Red dashed line shows the limit between preservation and degradation of the edifices. Compare pm03 vs. pc04 for example. Note that all pm's and pt's show evidence of degradation. The red arrow points to the only pc volcano with evidence of canyon erosion located at deeper waters.

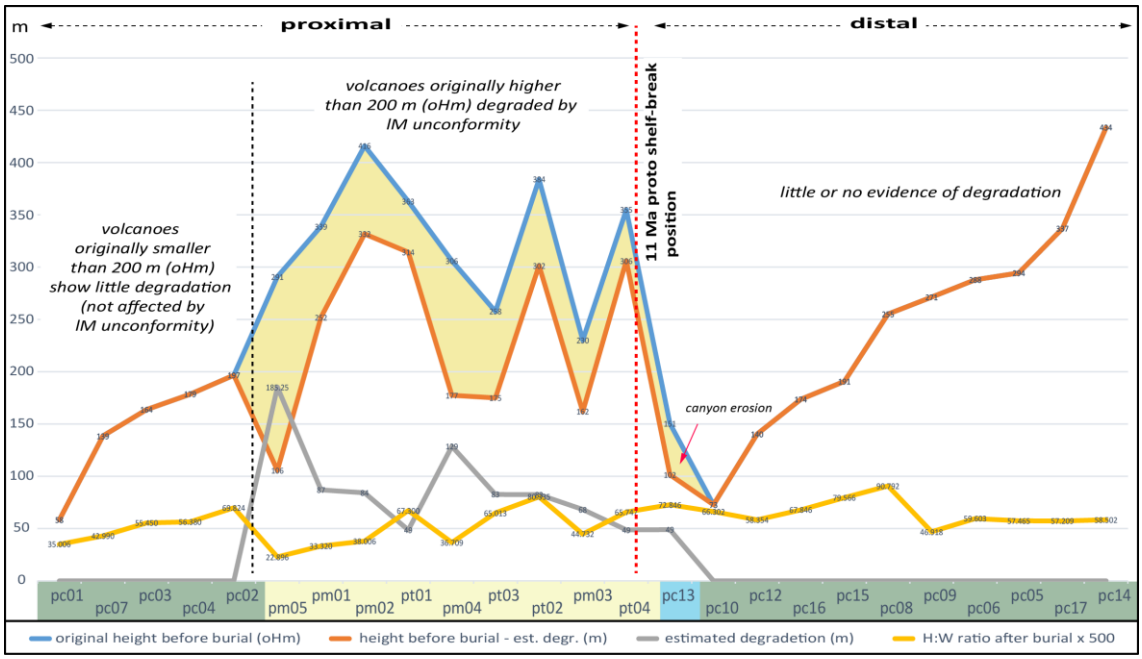

Figure 12: Morphometric analysis of cone-type dominated MVF volcanoes in relation to the lM unconformity. Data have been organized by the position of volcanoes relative to the 11 Ma shoreline (proximal and distal). They were then organized by the estimated degree of degradation from the highest to smallest values, and finally by oHm from smallest to highest values. The yellow fill represents volcanoes with a moderate to high degree of degradation. At the left-hand side of the graph, all volcanoes are pc's of < 200 m oHm and show little degradation. All pt's and pm's are located on the shelf at 11 Ma and have oHm > 200 m. We interpret that at ca 11 Ma, these volcanoes were volcanic islands and experienced wave erosion. All volcanoes located on the slope do not show significant evidence of degradation, with the exception of pm03 which was eroded by canyons. The H:W ratio was multiplied by 500 for visualization proposes. Note that the estimated degradation (grey) and the H:W (yellow) curves are inversely proportional, which indicates that a higher degree of degradation produced volcanoes with smaller H:W ratios, due to their loss in height (H) and gain in diameter (W).

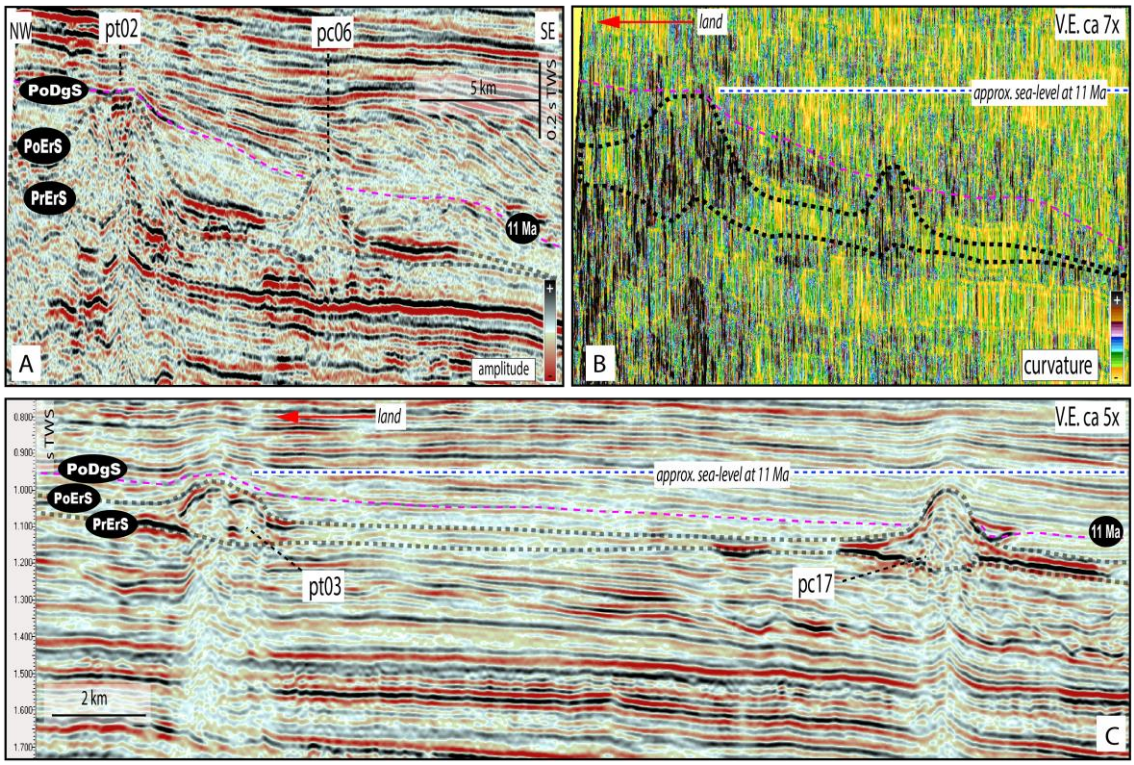

Figure 13: A and B show attribute analysis of pt02 and pc06 volcanoes and their seismic morphology. The curvature (B) attribute suggests that the internal and external parts of the volcanoes (black) are composed by rocks with similar acoustic properties, which are interpreted to represent volcanoclastic rocks eroded from the pt02 and deposited next to its flanks. C shows the morphological contrast between pt03 and pc17. Note that in both cases, extinct volcanic edifices located at shallow water (pt02 and pt03) show "flattened" tops in relation to the position of the 11 Ma unconformity, while volcanoes located at deeper water (pc06 and pc17) do not show a morphological relationship with this unconformity. This suggests that distal volcanoes were below sea-level and were well preserved. Blue dashed lines show the interpreted position of the sea-level at ca 11 Ma, based on the flattened top of proximal volcanoes.

References

Agirrezabala, L., Sarrionandia, F., Carracedo, M., 2017, Diatreme-forming volcanism in a deep-water faulted basin margin: Lower Cretaceous outcrops from the Basque-Cantabrian Basin, western Pyrenees. Journal of Volcanology and Geothermal Research. https://doi.org/10.1016/j.jvolgeores.2017.03.019

Barrier, .A., A. Nicol, A. P. Bischoff., 2017, Volcanism Occurrences in the Canterbury Basin, New Zealand and Implication for Petroleum Exploration. In AAPG GTW Influence of Volcanism and Associated Magmatic Processes on Petroleum Systems. Conference, Oamaru New Zealand.

Bischoff, A. P., A. Nicol, M. Beggs., 2017, Stratigraphy of architectural elements in a buried volcanic system and implications for hydrocarbon exploration: Interpretation, https://doi.org/10.1190/INT-2016-0201.1

Bischoff, A.P., 2019, Architectural Elements of Buried Volcanic Systems and Their Impact on Geoenergy Resources. Ph.D. Thesis, Canterbury University, New Zealand. Pre-print, 226p. https://doi.org/10.13140/RG.2.2.21440.58886

Blanke, S. J., 2010, "Saucer Sills" of the Offshore Canterbury Basin: GNS Publication, https://doi.org/10.1177/0094306114545742f

Cas, R. A. F., Landis, C. A., and Fordyce, R. E., 1989, A monogenetic, Surtla-type, Surtseyan volcano from the Eocene-Oligocene Waiareka-Deborah volcanics, Otago, New Zealand: A model: Bulletin of Volcanology, v. 51, no. 4, p. 281-298.

Cas, R., Satō, H., Simpson., C.J., 1993, Newer Volcanics province-processes and products of phreatomagmatic activity: Iavcei, Canberra 1993: excursion guide. Aust. Geol. Survey Organisation.

Cas, R. A. F., J. V. Wright., 1993, Volcanic Successions: Modern and Ancient - A Geological Approach to Processes, Products and Successions. Chapman and Hall, UK. https://doi.org/10.1007/978-0-412-44640-5

Cas, R. A. F., G. Giordano., 2014, Submarine volcanism: A review of the constraints, processes and products, and relevance to the Cabo de Gata volcanic succession: https://doi.org/10.3301/IJG.2014.46

Clague, D., R. Batiza., J.W. Head., A. Davis.,2000a, Pyroclastic and Hydroclastic Deposits on Loihi Seamount, Hawaii, in Explosive Subaqueous Volcanism, edited by J.D.L. White, J.L. Smellie, and D.A. Clague, American Geophysical

Union, Washington D.C., 200. Bulletin of Volcanology. https://doi.org/10.1029/140GM05

Clague, D. A., J. G. Moore., J. R. Reynolds., 2000b, Formation of Submarine Flat-Topped Volcanic Cones in Hawai'i. In: Explosive Subaqueous Volcanism, edited by J.D.L. White, J.L. Smellie, and D.A. Clague, American Geophysical Union, Washington D.C., 200. Bulletin of Volcanology. https://doi.org/10.1029/140GM05.doi:10.1007/s004450000088

Deardorff, N. D., K. V. Cashman., W. W. Chadwick., 2011, Observations of eruptive plume dynamics and pyroclastic deposits from submarine explosive eruptions at NW Rota-1, Mariana arc: Journal of Volcanology and Geothermal Research, https://doi.org/10.1016/j.jvolgeores.2011.01.003

Field, B.D., Browne, G.H., Davy, B.W., Herzer, R.H., Hoskins, R.H., Raine, J.I., Wilson, G.J., Sewell, R.J., Smale, D., Watters, W.A., 1989. Cretaceous and Cenozoic sedimentary basins and geological evolution of the Canterbury region, South Island, New Zealand. Lower Hutt: New Zealand Geological Survey. New Zealand Geological Survey basin studies 2. 94 p.

Fornaciai, A., M. Favalli., D. Karátson., S. Tarquini., E. Boschi., 2012, Morphometry of scoria cones, and their relation to geodynamic setting: A DEM-based analysis: Journal of Volcanology and Geothermal Research, https://doi.org/10.1016/j.jvolgeores.2011.12.012

Hansen, D. M., J. Cartwright., 2006, Saucer-Shaped Sill with Lobate Morphology Revealed by 3D Seismic Data: Implications for Resolving a Shallow-Level Sill Emplacement Mechanism. Journal of the Geological Society 163 (3): 509–23. https://doi.org/10.1144/0016-764905-073

Head, J. W., L. Wilson., 2003, Deep submarine pyroclastic eruptions: theory and predicted landforms and deposits: Journal of Volcanology and Geothermal Research, v. 121, no. 3, p. 155–193, https://doi.org/10.1016/S0377-0273(02)00425-0

Holford, S. P., N. Schofield, J. D. MacDonald, I. R. Duddy, P. F. Green., 2012, Seismic Analysis of Igneous Systems in Sedimentary Basins and Their Impacts on Hydrocarbon Prospectivity: Examples from the Southern Australian Margin. APPEA Journal, 52, 229–52.

Jackson, C. A.-L., 2012, Seismic reflection imaging and controls on the preservation of ancient sill-fed magmatic vents: Journal of the Geological Society, https://doi.org/10.1144/0016-76492011-147

Jutzeler, M., J. McPhie., S. R. Allen., 2014, Submarine eruption-fed and resedimented pumice-rich facies: the Dogashima Formation (Izu Peninsula, Japan): Bulletin of Volcanology, https://doi.org/10.1007/s00445-014-0867-x

Jones, A., D., G. Wilson., A. Gorman., B. Fox., D. Lee., U. Kaulfuss., 2017, A drill-hole calibrated geophysical characterisation of the 23 Ma Foulden Maar stratigraphic sequence, Otago, New Zealand: 1-13 p., https://doi.org/10.1080/00288306.2017.1369130

Kaulfuss, U., K. Németh, and J. White., 2012, Field Guide Miocene subaerial to subaqueous monogenetic volcanism in Otago, New Zealand.

Kereszturi, G., K. Németh., 2013, Monogenetic Basaltic Volcanoes: Genetic Classification, Growth, Geomorphology and Degradation: Updates in Volcanology - New Advances in Understanding Volcanic Systems, https://doi.org/10.5772/51387

Lorenz, V., 1985. Maars and diatremes of phreatomagmatic origin, a review. Transactions of the Geological Society of South Africa, 88: 459-470.: 459-470 p.

Magee, C., E. Hunt-Stewart., C. A. L. Jackson., 2013, Volcano growth mechanisms and the role of sub-volcanic intrusions: Insights from 2D seismic reflection data: Earth and Planetary Science Letters, https://doi.org/10.1016/j.epsl.2013.04.041

McLean, C. E., N. Schofield., D. J. Brown., D. W. Jolley., and A. Reid, 2017, 3D seismic imaging of the shallow plumbing system beneath the Ben Nevis Monogenetic Volcanic Field: Faroe–Shetland Basin: Journal of the Geological Society, https://doi.org/10.1144/jgs2016-118

Németh, K., 2010, Monogenetic volcanic fields; origin, sedimentary record, and relationship with polygenetic volcanism: Special Paper Geological Society of America, https://doi.org/10.1130/2010.2470(04)

Németh, K. and Kereszturi, G., 2015, Monogenetic volcanism: personal views and discussion. Int J Earth Sci (Geol Rundsch) 104: 2131. https://doi.org/10.1007/s00531-015-1243-6

Milne, A.D., 1975. Well completion report Resolution, for BP, Shell, Todd Canterbury Service Limited. New Zealand Geological Survey Open-file Petroleum Report No. 648.

Orton, G.J., 1996, Volcanic Environments. In Reading, H. G., 1996, Sedimentary Environments: Processes, Facies and Stratigraphy: 688 p.

Penna, R., Araujo, S., Sansonowski, R., Oliveira, L., Rosseto, J., Geisslinger, A. Matos, M., 2018, Igneous rock characterization through reprocessing, FWI imaging, and elastic inversion of a legacy seismic dataset in Brazilian Pre-Salt Province. 3277-3281. 10.1190/segam2018-2996032.1. https://doi.org/10.1190/segam2018-2996032.1

Planke, S., E. Alvestad, O. Eldholm., 1999, Seismic Characteristics of Basaltic Extrusive and Intrusive Rocks. The Leading Edge 18 (3): 342. https://doi.org/10.1190/1.1438289

Reynolds, P., N. Schofield., R. J. Brown., S. P. Holford., 2016, The architecture of submarine monogenetic volcanoes - insights from 3D seismic data: Basin Research, v. 30, p. 437–451, https://doi.org/10.1111/bre.12230

Reynolds, P., S., Holford, N. Schofield., A. Ross., 2017, Three-Dimensional Seismic Imaging of Ancient Submarine Lava Flows: An Example From the Southern Australian Margin: Geochemistry, Geophysics, Geosystems, https://doi.org/1002/2017GC007178

Schofield, N., D. A. Jerram., S. Holford., A. Stuart., M. Niall., A. Hartley., J. Howell., M. David., P. Green., D. Hutton., C. Stevenson., 2016, Sills in sedimentary basin and petroleum systems, in K. Németh, ed., The Series Advances in Volcanology, 1–22.

Silva, S. D., J. M. Lindsay., 2015, Primary Volcanic Landforms. The Encyclopedia of Volcanoes. https://doi.org/10.1016/B978-0-12-385938-9.00015-8

Schiøler, P., Raine, J.I., A. Griffin., C.J. Hollis., D.K. Kulhanek., H.E.G. Morgans., L. Roncaglia., C.P. Strong., C. Uruski., 2011. Revised biostratigraphy and well correlation, Canterbury Basin, New Zealand. GNS Science Consultancy Report 2011/12. 142 p.

Svensen, H., Planke, S., Malthe-Sorenssen, A., Jamtveit, B., Myklebust, R., Eidem, T.R., Rey,S.S., 2004, Release of methane from a volcanic basin as a mechanism for initial Eoceneglobal warming. Nature 429, 542–545

White, J. D. L., 2000, Subaqueous eruption-fed density currents and their deposits: Precambrian Research, 101 (2000) 87–109 https://doi.org/10.1016/S0301-9268(99)00096-0

White, J. D. L., J. L. Smellie., D. A. Clague., 2003, Introduction: A deductive outline and topical overview of subaqueous explosive volcanism, in Geophysical Monograph Series: https://doi.org/10.1029/140GM01

White, J. D. L., P. S. Ross., 2011, Maar-diatreme volcanoes: A review: https://doi.org/10.1016/j.jvolgeores.2011.01.010

White, J. D. L., C. I. Schipper., K. Kano., 2015a, Submarine Explosive Eruptions, in The Encyclopedia of Volcanoes: https://doi.org/10.1016/B978-0-12-385938-9.00031-6

White, J. D. L., J. McPhie., S. A. Soule., 2015b, Submarine Lavas and Hyaloclastite, in The Encyclopedia of Volcanoes: https://doi.org/10.1016/B978-0-12-385938-9.00019-5

White, J. D. L., G. A. Valentine., 2016, Magmatic versus phreatomagmatic fragmentation: Absence of evidence is not evidence of absence: Geosphere, https://doi.org/10.1130/GES01337.1

Wright, I. C., T. J. Worthington., J. A. Gamble., 2006, New multibeam mapping and geochemistry of the 30°-35° S sector, and overview, of southern Kermadec arc volcanism: Journal of Volcanology and Geothermal Research, https://doi.org/10.1016/j.jvolgeores.2005.03.021

Zimanowski, B., R. Büttner., V. Lorenz., H. G. Häfele., 1997, Fragmentation of basaltic melt in the course of explosive volcanism: Journal of Geophysical Research: Solid Earth, https://doi.org/10.1029/96JB02935

Zimanowski, B., R. Büttner., 2003, Phreatomagmatic explosions in subaqueous volcanism, in Geophysical Monograph Series: https://doi.org/10.1029/140GM03